Bull. Mater. Sci., Vol. 39, No. 7, December 2016, pp. 1801–1808. © Indian Academy of Sciences.
DOI 10.1007/s12034-016-1335-3

Structural, dielectric and a.c. conductivity study of Sb_2O_3 thin film obtained by thermal oxidation of Sb_2S_3

M HAJ LAKHDAR[1,*], T LARBI[1], B KHALFALLAH[2], B OUNI[1] and M AMLOUK[1]
[1]Unité de Physique des Dispositifs a Semi-Conducteurs, Faculté des Sciences de Tunis, Université de Tunis El Manar, 2092 Tunis, Tunisia
[2]Laboratoire de Photovoltaïque et Matériaux Semiconducteurs, Ecole Nationale d'Ingénieurs de Tunis, Université de Tunis El Manar, 2092 Tunis, Tunisia

MS received 12 March 2016; accepted 18 May 2016

Abstract. **This work highlights some physical properties of Sb_2O_3 thin films obtained through heat treatment of Sb_2S_3 thin films under an atmospheric pressure at 400°C. The obtained material is characterized by X-ray diffraction and impedance spectroscopy. X-ray diffraction analysis shows that Sb_2O_3 thin films were crystallized in cubic structure having a preferential growth along (222) plane. The grain size is found to be around 65 nm. The electrical conductivity was studied using impedance spectroscopy technique in the frequency range from 5 Hz to 13 MHz at temperatures lying in 638–698 K domain. Besides, the frequency and temperature dependence of the complex impedance, a.c. conductivity and complex electric modulus have been investigated.**

Keywords. **X-ray diffraction; a.c. conductivity; dielectric properties; complex electric modulus.**

1. Introduction

Oxide semiconductors occur in wide range of crystalline structures and have various electrical and optical properties, in particular the coexistence of both transparency and conductivity [1,2]. Antimony trioxide exists in two crystalline structures: senarmontite (cubic phase) and valentinite (orthorhombic phase). Moreover, Sb_2O_3 is a wide-band-gap material and could be used with other oxides in various applications [3–5]. The electrical conductivity characterization and optimization in oxide thin films and nanostructures is an important step for application in electronics and optoelectronics [6]. It is widely believed that the possible causes of the often observed conductivity in the oxides are due to oxygen vacancies, cation interstitial or to the incorporation of impurities [7,8]. In recent years, attention has been paid to the study disordered systems because of the unusual temperature dependence of their conductivity [9]. In polycrystalline materials, the charge carrier transport can occur via hopping between localized states. In fact, Landau and Lifchitz [10] introduced the concept of polaron and its spatial extension to modulate the electronic energy levels in the potential well created by the polarization of the crystal lattice. AC conductivity measurements have been widely used to investigate the frequency and the temperature dependences of the a.c. conductivity, dielectric constant and dielectric loss with a view to understand the conduction mechanism involved in polycrystalline structure of many oxides [11–13]. As previously reported, several studies show that the real part of the a.c. conductivity as a function of frequency and temperature of various oxides elaborated in our laboratory obeys the universal power law of Jonscher [14–19]. According to the literature, several researchers studied the structural, optical and electrical properties of antimony oxide. However, to date, no reports have appeared on impedance spectroscopy, modulus behaviour, electrical conductivity, dielectric relaxation and dielectric properties of crystalline Sb_2O_3 thin films. This article deals for the first time with the frequency and temperature dependences of a.c. conductivity and complex electric modulus in order to identify conduction mechanism in Sb_2O_3 thin films.

2. Experimental

2.1 *Sb_2O_3 thin films*

Sb_2O_3 thin films have been prepared in three stages. First, thin films of Sb (99.98% of purity) were obtained by evaporation in HV chamber using a relatively low pressure of the order of 10^{-4} to 10^{-5} Pa. The films were deposited on 1×2 cm^2 glass substrates at substrate temperature Ts = 100°C. The typical deposition parameter of this metal corresponds to a growth rate of $1\,nm\,s^{-1}$. The thickness of antimony thin films was subject to change by means of varying the deposition time and the mass of Sb element. Second, Sb thermal evaporated thin films were placed into pyrex presealed in the presence of sulphur grains (99.98% of purity). After that, the sample was heated under vacuum (10^{-3} Pa) at a rate of $10\,K\,min^{-1}$ from room temperature up to 300°C for 6 h using a programmed tubular oven. Then, the samples

*Author for correspondence (hajlakhdarmourad@gmail.com)

were cooled down [20]. Finally, the as-obtained Sb_2S_3 thin films were annealed at 400°C in air atmosphere for 6 h inside the same oven. Thus, new Sb_2O_3 thin films were obtained.

2.2 *Characterization techniques*

Structural analysis were performed by X-ray diffraction technique (Analytical X'Pert PROMP D) with CuKα radiation as source having wavelength $\lambda = 1.54056$ Å. The impedance meter (Hewlett-Packard 4192 analyzer) has been used to reach the electrical conductivity of Sb_2O_3 thin films in the frequency range 5 Hz to 13 MHz at various temperatures (638–698 K). The electrical measurement was conducted using two shaped electrodes of band painted on either end of the sample by using the silver paste. AC conductivity was obtained from $\sigma_{\text{a.c.}} = \ell/Z'S$, where Z' is the real component of the complex impedance, ℓ the distance between electrodes and S the cross-sectional area.

3. Results and discussion

3.1 *Structural study*

XRD patterns were used to reach the structural states of Sb_2O_3 thin films. In figure 1, all peaks match well with the standard pattern of cubic Sb_2O_3 material (PDF 01-072-1334). These peaks are assigned to (111), (400), (444) and (222) directions. The as-synthesized Sb_2O_3 thin film exhibits polycrystalline nature with cubic crystal structure having a preferential growth along (222) plane. This structural study is consistent with those reported previously [3,21–24]. In fact, X-ray diffraction profiles can be used to calculate the grain size D, lattice parameter (a), dislocation density (δ) and the microstrain (ε), which played important roles in optical, electrical and mechanical properties of a material.

Also, the interplanar spacing d_{hkl} values of Sb_2O_3 thin films were calculated from Bragg equation. The cubic lattice parameter (a) for the cubic phase structure is determined via (111), (400), (444) and (222) orientations using the following relation:

$$d_{hkl} = \frac{a}{\sqrt{h^2 + k^2 + l^2}}. \tag{1}$$

The value of lattice parameters (a) estimated from equation (1) is found to be 1.105 nm, which is consistent with the standard value for powder cubic Sb_2O_3 ($a = 1.113$ nm). The grain size D value is estimated from (222) diffraction line of Sb_2O_3 thin film using Debye–Scherer formula:

$$D = \frac{K\lambda}{\beta \cos\theta}, \tag{2}$$

where K is a constant equal to 0.9 and β the width at half-maximum related to the crystallite size. The grain size is found to be around 64.6 nm.

The dislocation density is estimated using:

$$\delta = \frac{1}{D^2}. \tag{3}$$

Its value is found to be around 2.39×10^{14} lines m^{-2}.

In the same line, the microstrain (ε) of Sb_2O_3 thin film was calculated from:

$$\varepsilon = \frac{\beta}{4\tan\theta}. \tag{4}$$

The value of the microstrain (ε) is of the order of 1.27×10^{-3}.

These structural parameters calculated above maybe of interest to understand and to discuss the electrical conduction mechanisms inside thin film of antimony oxide, as detailed in the next section.

3.2 *Impedance analysis*

The complex impedance (Z'' *vs.* Z') plots of Sb_2O_3 thin films at different temperatures are displayed in figure 2. In the temperature range investigated, complex curve consists only

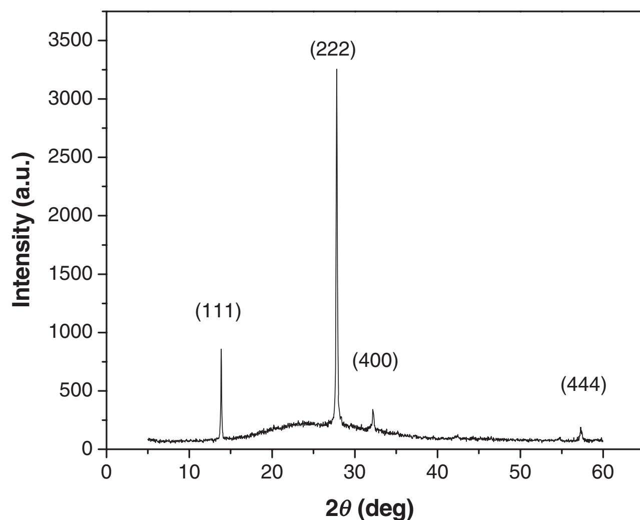

Figure 1. XRD spectra of Sb_2O_3 thin films.

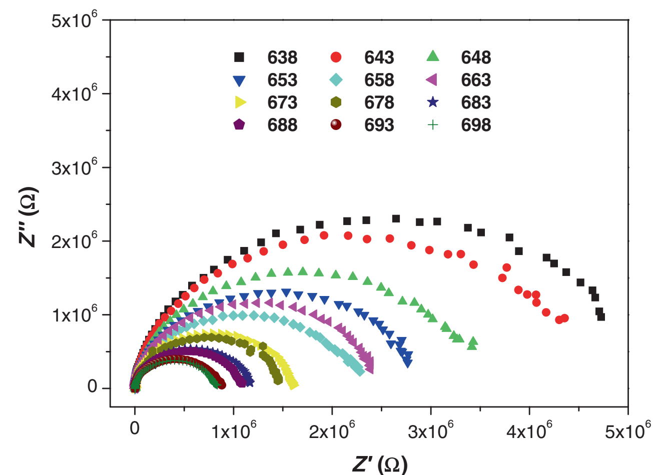

Figure 2. Complex impedance spectra at different temperatures.

one depressed semi-circle and its centre lies below the real axis. Furthermore, depressed arc is typical for a dipolar system involving distribution of relaxation time [25]. Moreover, it is noted that the diameter of semi-circles decreases with increase in temperature referring to pronounced decrease in the resistivity. These characteristics are attributed to a semiconductor behaviour, in which the electrical conduction process is thermally activated. The equivalent circuit for the depressed semi-circles of this polycrystalline thin film may be described by a parallel connection of an ohmic resistor R and a constant phase element (CPE). Indeed, in the present study, the complex plane plot can be described by Cole–Cole model, which is given by [26]:

$$Z = \frac{R}{[1 + (j\omega\tau)^{\alpha}]}, \tag{5}$$

where ω is angular frequency, $\tau = \text{RC}$ is the relaxation time and α a parameter that characterizes the distribution of relaxation times with values ranging from 0 to 1. For Debye relaxation, $\alpha = 0$ and $\alpha > 0$ for the case where relaxation times have distribution. The real and imaginary parts of equation (5) are as follows:

$$Z' = \frac{R\left[1 + (\omega\tau)^{\alpha}\sin\left((1-\alpha)\pi/2\right)\right]}{\left[1 + 2(\omega\tau)^{\alpha}\sin\left((1-\alpha)\pi/2\right) + (\omega\tau)^{2\alpha}\right]}, \tag{6}$$

$$Z'' = \frac{R\left[(\omega\tau)^{\alpha}\cos\left((1-\alpha)\pi/2\right)\right]}{\left[1 + 2(\omega\tau)^{\alpha}\sin\left((1-\alpha)\pi/2\right) + (\omega\tau)^{2\alpha}\right]}. \tag{7}$$

Figure 3 shows the experimental values of Z' *vs.* frequency at different temperatures. The solid line represents best fit to experimental data according to equation (6). As seen in figure 2, Z' magnitude decreases with increase in both the frequency and temperature, which indicates a semiconductor behaviour.

Imaginary parts of complex impedance (Z'') *vs.* frequency at different temperatures are shown in figure 4. Solid line represents indeed the best fit to experimental data according to equation (7). We note that, as the temperature increases, the imaginary part (Z'') increases with increase in frequency reaching a maximum peak $(Z''_{\max})$ and then decreases. Moreover, when the temperature increases, the position of the relaxation peak shifts to higher frequencies, we also note that the value of $Z''_{\max}$ decreases. It is also known that the relaxation time (τ) can be deduced from the peaks corresponding to (Z'') following equation (8):

$$\tau = \frac{1}{2\pi f_Z}. \tag{8}$$

The variations of the temperature with relaxation frequency (f_Z) corresponding to the maximum of (Z'') are shown in the inset of figure 4. Solid line represents best fit to experimental data according to Arrhenius law given by [27]:

$$f_Z = f_0 \exp\left(-\frac{E_{aZ}}{k_B T}\right), \tag{9}$$

where E_{aZ} is the activation energy, f_0 the pre-exponential factor, T the measured temperature and k_B the Boltzmann constant. The activation energy is calculated from straight line fit to equation (9). Its value is around 1.23 eV.

In the same way, figure 5 shows a master plot of the imaginary parts of complex impedance at different temperatures, where frequency axis is normalized by (f_Z) and (Z'') axis by $(Z''_{\max})$. The matching of curves at various temperatures into a single curve indicates that the dynamical processes occurring at different frequencies are independent of temperature.

3.3 *Conductivity study*

Figure 6 shows the plots of $\ln(\sigma_{a.c.})$ *vs.* frequency at various temperatures for Sb_2O_3. It is found that the conductivity is substantially constant at low frequencies while at higher frequencies it increases rapidly. On the other hand, the conductivity shows dispersion which shifts to higher frequency side with the increase in temperature.

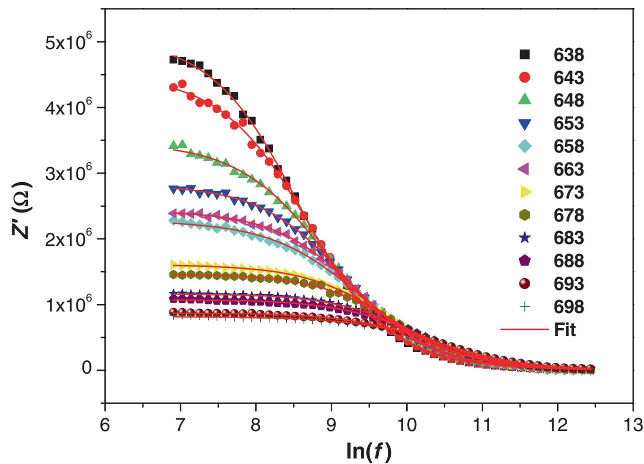

Figure 3. Frequency dependence of Z' at different temperatures.

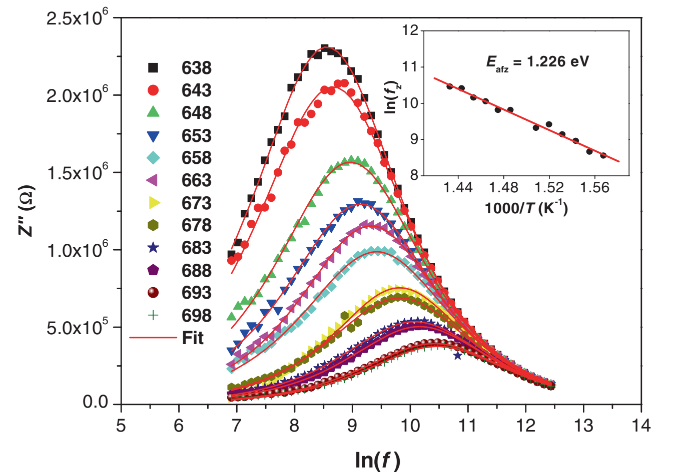

Figure 4. Frequency dependence of Z'' at different temperatures. Inset: temperature dependence of relaxation frequency for Z''.

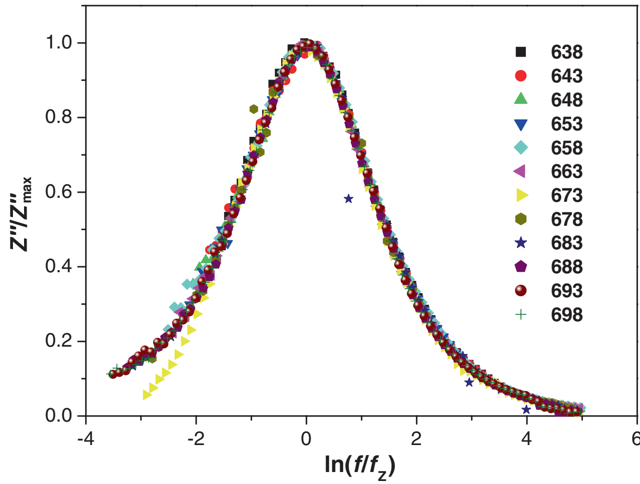

Figure 5. Variation of $Z''/Z''_{\max}$ with $\ln(f/f_Z)$ at different temperatures.

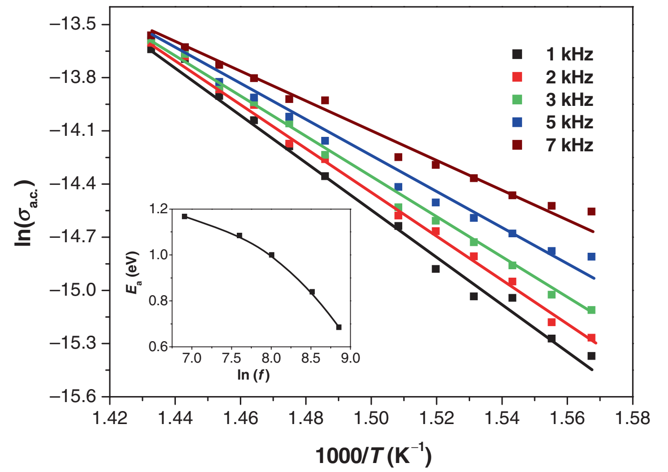

Figure 7. Temperature dependence of a.c. conductivity at different frequencies. Inset: frequency dependence of a.c. activation energy.

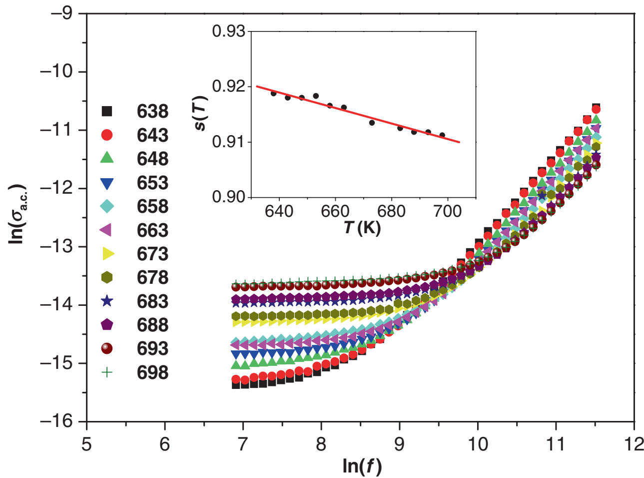

Figure 6. Frequency dependence of a.c. conductivity at different temperatures. Inset: temperature dependence of the parameter s.

The variation of conductivity with angular frequency at different temperatures can be analysed within the framework of the Jonscher's universal power law [28]:

$$\sigma_{\text{a.c.}} = \sigma_{\text{d.c.}} + A\omega^{s}, \tag{10}$$

where ω is the angular frequency, A a constant determining the strength of the polarizability, $\sigma_{\text{d.c.}}$ the d.c. conductivity due to band conduction and (s) is an exponent lower or equal to unity, which has an important physical meaning [29]. From the slope of the linear part at high frequencies of the variation of the conductivity with angular frequency at different temperatures, we determined the different values of the exponent (s) for different temperatures. Various theoretical models for a.c. conductivity have been proposed to reproduce the temperature dependence of (s). The quantum mechanical tunnelling suggests that (s) is temperature independent [30]. According to the overlapping large polaron tunnelling model suggested by Wang *et al* [31], (s) should decrease with increase in the temperature up to a certain temperature, after that, (s) increases with further increase in the temperature. In the case of small polaron model, (s) should increase with increase in the temperature [32]. For the sake of clarity, the variation of (s) with temperature for the sample under investigation is shown in the inset of figure 6. It is still remarkable that the value of (s) decreases with the increase of the temperature. Such behaviour proves that the conduction mechanism can be modelled by the correlated barrier hopping (CBH). In the CBH model, the charge carriers hop indeed between the sites over a potential barrier separating them. The expression for (s) derived on the basis of this model is given by Elliott [33,34]:

$$s = 1 - \frac{6k_{\text{B}}T}{E_{\text{g}}}, \tag{11}$$

where E_{g} is the bandgap energy of the material at room temperature, which is about 3.7 eV.

Figure 7 shows the variation of a.c. conductivity with temperature at different frequencies. As seen from this figure, a.c. conductivity increases linearly with $1000/T$. Such behaviour suggests that a.c. conductivity is thermally activated from different localized states in the bandgap [35]. Furthermore, a.c. conductivity *vs.* temperature, at different frequencies, can be modelled by the Arrhenius law given by:

$$\sigma_{\text{a.c.}} = \sigma_{\text{a.c.0}} \exp\left(-\frac{E_{\text{a.c.}}}{k_{\text{B}}T}\right). \tag{12}$$

Frequency dependence of a.c. activation energy is shown in the inset of figure 7. It is still remarkable that the activation energy decreases with increase in frequency, this behaviour can be explained by the contribution of the frequency to the conduction mechanism, which further confirms that the dominant mechanism is the hopping conduction process.

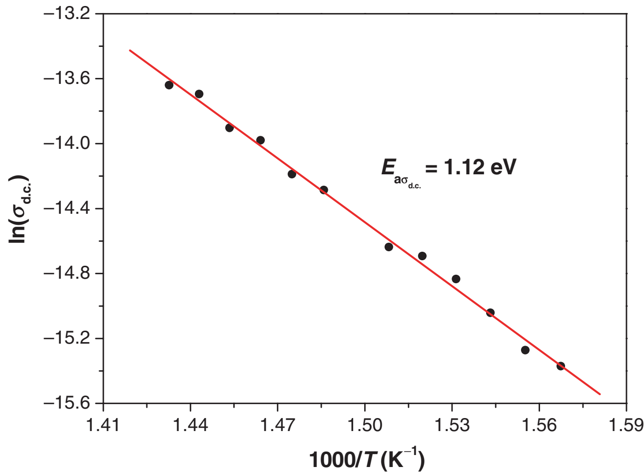

Figure 8. Temperature dependence of d.c. conductivity.

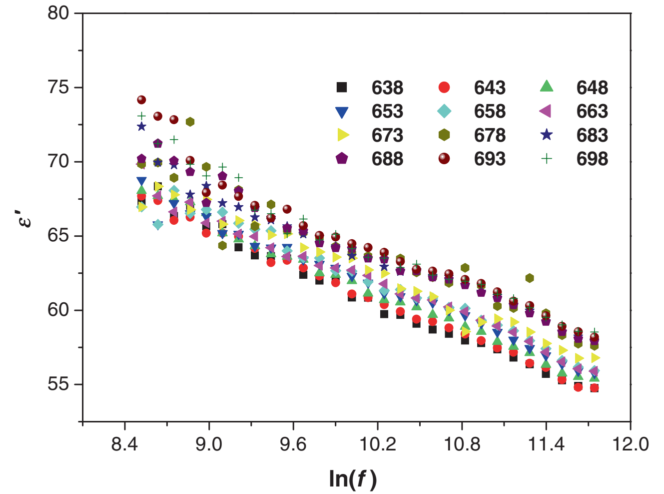

Figure 9. Frequency dependence of dielectric constant at different temperatures.

As plotted in figure 8, d.c. conductivity satisfies the Arrhenius law which can be written as:

$$\sigma_{\text{d.c.}} = \sigma_{\text{d.c.0}} \exp\left(-\frac{E_{\text{d.c.}}}{k_{\text{B}}T}\right), \tag{13}$$

where $\sigma_{\text{d.c.0}}$ is the pre-exponential factor and $E_{\text{d.c.}}$ the activation energy for d.c. conduction. We note a value of activation energy of about 1.12 eV, which is almost identical to the activation energy obtained from the angular relaxation frequency.

3.4 *Dielectric study*

The study of dielectric properties is another important source of information on the conduction process. This study can be used to explain the origin of dielectric losses, electrical and dipolar relaxation time.

Figure 9 shows the frequency dependence of dielectric constant at different temperatures. First, at constant temperature, the dielectric constant decreases by increase in frequency of the applied field. This behaviour can be assigned to the fact that at low frequencies, several kinds of polarizations contribute to the dielectric constant value, as deformational polarization (electronic, ionic) as well as relaxation (orientational and interfacial). When the frequency becomes higher, the electric dipoles can no longer follow the variation of the electric field, which leads to a reduction of orientational polarization. At high frequency, ε' reaches a constant value due to interfacial polarization. On the other hand, at a constant frequency, the dielectric constant increases by increase in the temperature. This behaviour can be explained by the fact that the dipoles cannot orient themselves at low temperatures. When the temperature increased, the orientation of dipoles is facilitated (following thermal movements), which tends to an increase in dielectric constant value.

Furthermore, the dielectric loss is given by:

$$\tan\delta = \frac{Z''}{Z'}. \tag{14}$$

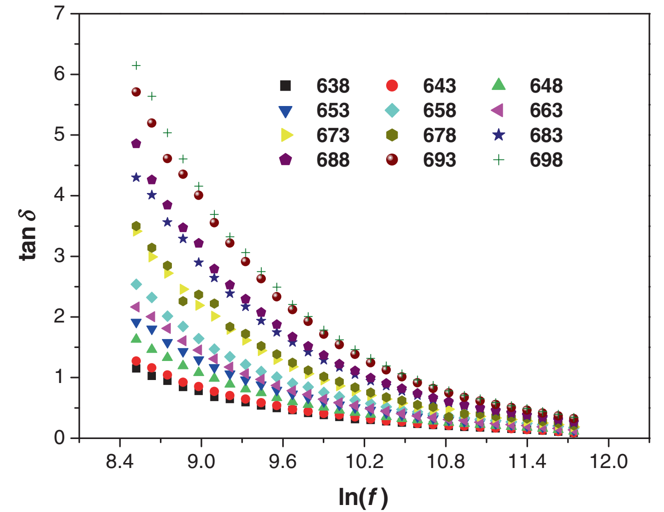

Figure 10. Frequency dependence of dielectric loss at different temperatures.

The variation of the dielectric loss with the frequency at different temperatures of Sb_2O_3 thin films is shown in figure 10. At constant frequency, the dielectric loss increases by increase in temperature. This behaviour can be explained by the fact that at low temperatures, the conduction loss is minimal, when the temperature increases the conduction loss increases due to the increase in conductivity [36]. This increases the value of dielectric loss with increase in temperature.

3.5 *Electric modulus study*

The impedance spectrum does not provide information at high and low frequencies. Another approach to study electrical relaxation of material is the complex electrical modulus M^* [37]. The real M' and imaginary M'' parts of electric

modulus were calculated from the impedance data using the following relation:

$$M^* = M' + jM'' = j\omega C_0 Z^*, \tag{15}$$

where $C_0 = \varepsilon_0 S/d$ is the empty cell capacitance, ε_0 represents the permittivity of free space, d the sample thickness and S the area of the sample.

Figure 11 shows M'' *vs.* M' plots. It is found that the M'' *vs.* M' plots at different temperatures overlap on a single arc indicating the presence of a single phase of the material. This result is in good agreement with the structural study. Furthermore, figure 11 reveals that the semi-circles are depressed and their centres are shifted down to M' axis. This behaviour is related to distributions of relaxation time, which supports the non-Debye type of relaxation in this material.

The variations of the real parts of the electric modulus M' as a function of frequency at different temperatures are shown in figure 12. We note that M' value approaches zero for low frequency. This behaviour can be assigned to a lack of force, which governs the mobility of charge carriers under the influence of an electric field [38]. Furthermore, an increase in the M' value with increase in frequency at different temperatures has been observed.

The variations of imaginary parts with frequency at different temperatures are plotted in figure 13. It is seen that M'' increases with frequency and reaches a maximum value, and then decreases. On the other hand, the position of the relaxation peak shifts to higher frequencies with increase in temperature. In the region to the right of the peak, the charge carriers may be considered as confined to potential wells and free to move within the wells, while to the left of the peak, the charge carriers are mobile over long distances. So, the region of peak frequency represents the transition from long mobility range to short range one [39].

In order to determine some characteristic parameters of the charge carriers such as their activation energy and relaxation frequency, we have fitted the imaginary parts of the electric modulus for different temperatures, with an approximate frequency representation of the Kohlrausch Williams Watts (KWW) function, proposed by Bergman [40]:

$$M''(f) = \frac{M''_{\mathrm{p}}(f)}{1-\beta+[\beta/(1+\beta)]\left[\beta\left(f_{\mathrm{p}}/f\right)+\left(f/f_{\mathrm{p}}\right)^{\beta}\right]}, \tag{16}$$

where M''_{p} is the peak maximum, f_{p} the peak frequency of imaginary part of the modulus and β the well-known Kohlrausch parameter. This parameter characterizes the degree of non-Debye behaviour ($0 \le \beta \le 1$, $\beta = 1$ for Debye relaxation). In this study, the value of $\beta < 1$ suggests that the non-Debye type of relaxation prevails in these samples.

Figure 14 shows the variation of relaxation frequency with temperature, which follows Arrhenius relation:

$$f_{\mathrm{M}} = f_{0\mathrm{M}} \exp\left(-\frac{E_{\mathrm{aM}}}{k_{\mathrm{B}}T}\right), \tag{17}$$

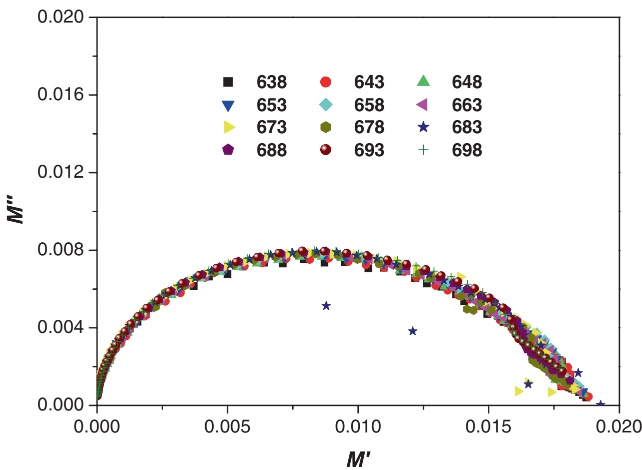

Figure 11. Complex modulus spectrum at different temperatures.

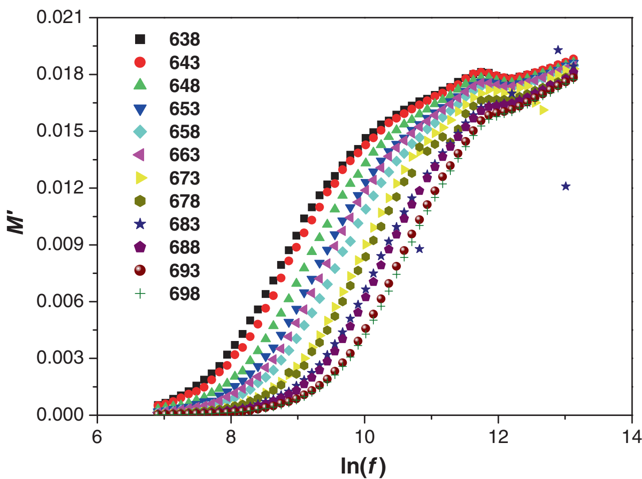

Figure 12. M' frequency dependence at different temperatures.

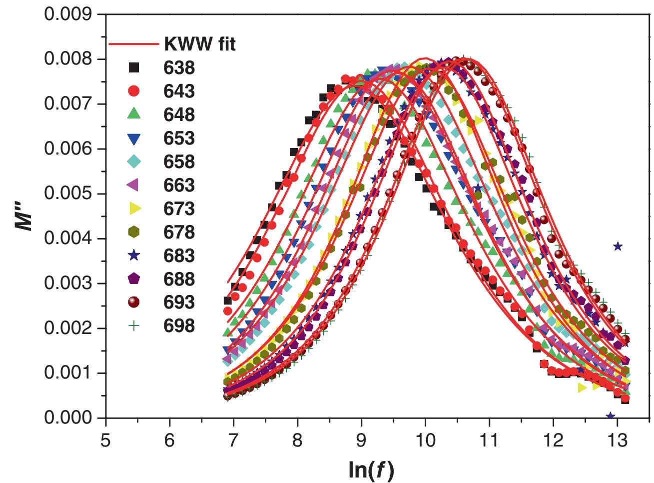

Figure 13. M'' frequency dependence at different temperatures.

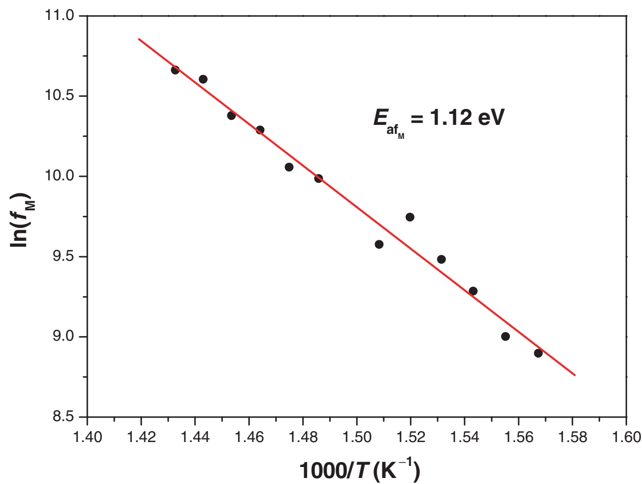

Figure 14. Temperature dependence of relaxation frequency for M''.

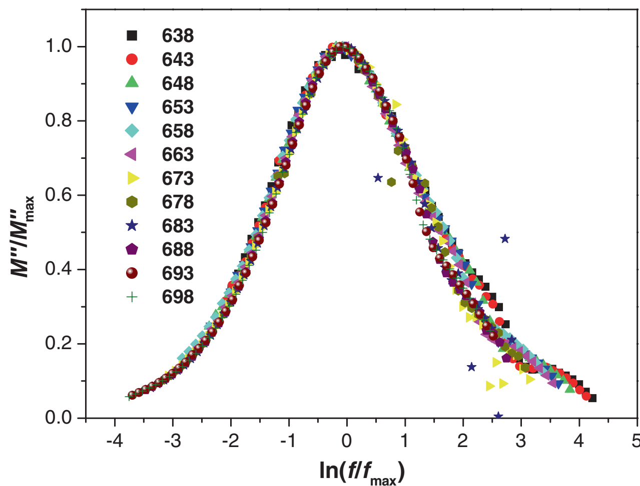

Figure 15. Variation of M''/M''_{max} with $\ln(f/f_M)$ at different temperatures.

where E_{aM} is the activation energy for dielectric relaxation and f_{0M} the pre-exponent factor. We note that the value of E_{aM} was found to be around 1.12 eV.

Moreover, figure 15 displays the variation of M''/M''_{max} with $\ln(f/f_M)$ at different temperatures. The overlap of the curves for all temperatures indicates that the relaxation shows the same mechanism at various temperatures.

The variation of normalized parameters M''/M''_{max} and Z''/Z''_{max} with frequency is plotted in figure 16. It is known that the overlapping peak position of M''/M''_{max} and Z''/Z''_{max} gives an idea about relaxation (delocalized or long range) [41]. For Sb_2O_3 the M''/M''_{max} and Z''/Z''_{max} peaks do not overlap, which proves the existence from both long range and localized relaxation. On the other hand, the broadenings of both Z'' and M'' spectra may be due to the existence of a distribution of relaxation times [42].

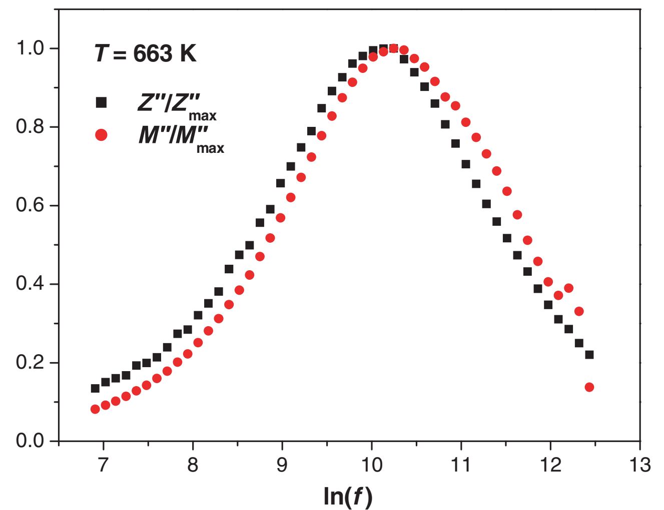

Figure 16. Variation of normalized parameters M''/M''_{max} and Z''/Z''_{max} with frequency.

4. Conclusion

This study covers some electrical properties of Sb_2O_3 ceramic thin films obtained through thermal treatment of Sb thin films under a sulphur atmosphere at 300°C followed by an oxidation step in air for 6 h at 400°C. Dielectric relaxation, modulus behaviour and conduction mechanism of obtained Sb_2O_3 thin films have been investigated in terms of both temperature and frequency. The study of a.c. conductivity via frequency at different temperatures found to obey the Jonscher's universal power law dependence. The scaling behaviour of imaginary impedance and imaginary electric modulus suggests that the relaxation phenomenon describes the same mechanism at various temperatures. Further studies are in progress to test this binary oxide in some sensitive and electronic devices.

References

[1] Gupta Sushant, Yadav B C, Dwivedi P K and Das B 2013 *Mater. Res. Bull.* **48** 3315

[2] Ouni B, Ouerfelli J, Amlouk A, Boubaker K and Amlouk M 2010 *J. Non-Cryst. Solids* **356** 1294

[3] Tigau N, Ciupina V and Prodan G 2005 *J. Cryst. Growth* **277** 529

[4] Sun Q, Ren Q Q, Li H and Fu Z W 2011 *Electrochem. Commun.* **13** 462

[5] Nalin M, Messaddeq Y, Ribeiro S J L, Poulain M and Briois V 2001 *J. Optoelectron. Adv. Mater.* **3** 553

[6] Zhang Z, Bian J, Sun J, Ma X, Wang Y, Cheng C *et al* 2012 *Mater. Res. Bull.* **47** 2685

[7] Janotti A and Van de Walle C G 2009 *Rep. Prog. Phys.* **72** 126501 (29pp)

[8] Larbi T, Haj Lakhdar M, Amara A, Ouni B, Boukhachem A, Mater A and Amlouk M 2015 *J. Alloys Compd.* **626** 93

[9] Díaz-Guillén M R, Díaz-Guillén J A, Fuentes A F, Santamaría J and León C 2010 *Physical Rev. B* **82** 174304

[10] Landau L and Lifchitz E 1969 *Electrodynamique des milieux continus* chapter IX 325 Edition Mir, Moscow

[11] Parthasrathy G, Naik G M and Asokan S 1987 *J. Mater. Sci. Lett.* **6** 181

[12] Ouni B, Haj Lakhdar M, Boughalmi R, Larbi T, Boukhachem A, Madani A *et al* 2013 *J. Non-Cryst. Solids* **367** 1

[13] HajLakhdar M, Larbi T, Ouni B and Amlouk M 2015 *Mater. Sci. Semicond. Process.* **40** 596

[14] Larbi T, Ouni B, Boukachem A, Boubaker K and Amlouk M 2014 *Mater. Sci. Semicond. Process.* **22** 50

[15] Arfaoui A, Ouni B, Touihri S and Mannoubi T 2014 *Mater. Res. Bull.* **60** 719

[16] Larbi T, Amara A, Ben Said L, Ouni B, Haj Lakhdar M and Amlouk M 2015 *Mater. Res. Bull.* **70** 254

[17] Boukhachem A, Bouzidi C, Boughalmi R, Ouerteni R, Kahlaoui M, Ouni B *et al* 2014 *Ceram. Int.* **40** 13427

[18] Mhamdi A, Ouni B, Amlouk A, Boubaker K and Amlouk M 2014 *J. Alloys Compd.* **582** 810

[19] Arfaoui A, Ouni B, Touihri S, Mhamdi A, Labidi A and Manoubi T 2015 *Opt. Mater.* **45** 109

[20] Haj Lakhdar M, Ouni B and Amlouk M 2014 *Optik* **125** 2295

[21] Zhang L, Pan C-L and Liu Y 2012 *Mater. Lett.* **75** 29

[22] Changhui Ye, Meng G, Zhang L, Wang G and Wang Y 2002 *Chem. Phys. Lett.* **363** 34

[23] Zeng D W, Zhu B L, Xie C S, Song W L and Wang A H 2004 *Mater. Sci. Eng. A* **366** 332

[24] Ma X, Zhang Z, Li X, Du Y, Xu F and Qian Y 2004 *J. Solid State Chem.* **177** 3824

[25] Haj Lakhdar M, Ouni B and Amlouk M 2014 *Mater. Sci. Semicond. Process.* **19** 32

[26] Cheruku R, Vijayan L and Govindaraj G 2012 *Mater. Sci. Eng. B* **177** 771

[27] Hill R M and Jonscher A K 1979 *J. Non-Cryst. Solids* **32** 53

[28] Jonscher A K 1977 *Nature* **267** 673

[29] Funke K 1993 *Prog. Solid State Chem.* **22** 111

[30] Jung W H 2008 *Physica B* **403** 636

[31] Wang K, Chen H and Shen W Z 2003 *Physica B* **336** 369

[32] Abdelmoneim H M 2010 *Acta Phisica Polonica A* **117** 936

[33] Elliott S R 1978 *Philos. Mag. B* **36** 1291

[34] Elliott S R 1978 *Philos. Mag. B* **37** 135

[35] Pike G E 1972 *Phys. Rev. B* **6** 1572

[36] Farid A M and Bekheet A E 2000 *Vacuum* **59** 932

[37] Macedo P B, Moynihan C T and Bose R 1972 *Phys. Chem. Glasses* **13** 171

[38] Prabu M and Selvasekarapandian S 2012 *Mater. Chem. Phys.* **134** 366

[39] Dult M, Kundu R S, Hooda J, Murugavel S, Punia R and Kishore N 2015 *J. Non-Cryst. Solids* **423** 1

[40] Vijayan L, Cheruku R, Govindaraj G and Rajagopan S 2011 *Mater. Chem. Phys.* **125** 184

[41] Gerhardt R 1994 *J. Phys. Chem. Solids* **55** 1491

[42] Almond D P and West A R 1983 *Solid State Ionics* **11** 57